RESISTANCE WELDING OF LOW-MELT POLYARYLETHERKETONE: PROCESS DEFINITION AND OPTIMIZATION

Manuel Endrass[a], Anton Thomé[a], Victor Gadletz[b], Simon Bauer[a], Stefan Jarka[a], Philipp Gänswürger[a], Frederic Fischer[a], Stefan Ferstl[b], Lars Larsen[a] and Michael Kupke[a]

a: Institute of Structures and Design (IBT), Center for Lightweight Production Technology (ZLP), German Aerospace Center (DLR), Am Technologiezentrum 4, D - 86159 Augsburg – manuel.endrass@dlr.de
b: Premium AEROTEC GmbH, Haunstetter Str. 225, D - 86179 Augsburg

Abstract: *Within the European Clean Sky 2 Program thermoplastic composites are readied for future single aisle application and validated by the full-scale demonstration of the so-called Multifunctional Fuselage Demonstrator (MFFD). DLR together with Premium AEROTEC, AERNnova and AIRBUS will deliver the upper half shell for this 8 m long barrel made of carbon fiber-reinforced low-melt Polyaryletherketone (LM-PAEK). Resistance welding was chosen to join the C-frames with up to 19 attached flanges of varying length to the fuselage skin. For process definition, the welding parameters of LM-PAEK were investigated using a customized weld module. The main processing parameters affecting the quality of the weld, were defined as input parameters for a Design of Experiments (DoE). The DoE was conducted on the basis of a glass-insulated welding element. The bondline quality of each parameter set (design point) was assessed by water-coupled ultrasonic investigations, the fracture load values defined by single lap shear testing and microscopic fracture surface analyses. Thus, a numerical parameter optimization was performed in order to define the weld parameters for frame integration. Within a second evolution stage of the welding elements, replacing the glassfiber insulation of the welding elements to pure resin films, the potentials for a mechanical performance increase could be demonstrated.*

Keywords: Clean Sky 2, Resistance Welding, LM-PAEK, Design of Experiments, Non-Destructive- & Destructive-Testing

1. Introduction

State-of-the-art aircraft assembly is a mainly sequential process, where the installation of systems and cabin interior monuments is strictly separated from the prior structure assembly. The possibility for re-organizing the aircraft assembly sequence with pre-equipped modules (already containing cabin and systems installations) due to dustless joining technologies for carbon fiber-reinforced high-performance thermoplastics (CFR-TP`s) can be named as game changing opportunity on the reduction of lead time for the aircraft manufacturing. The German Aerospace Center`s (DLR) Center for Lightweight Production Technology (ZLP) Augsburg, together with Premium AEROTEC (PAG), Airbus and AERNnova are responsible for the component manufacturing and assembly of the Multifunctional Fuselage Demonstrators (MFFD) eight-meter long upper shell structure made from Toray Advanced Composites TC 1225 LM-PAEK within the framework of Clean Sky 2.

In-Situ tape placement (skin manufacturing), continuous ultrasonic (stringer integration) and resistance welding (frame, frame-coupling and cleat integration) are matured, modified and adapted towards a safe and sound process execution within the upper shell structure manufacturing. This paper focusses on the process definition and optimization of resistance welding of LM-PAEK as intermediate project milestone, based on the use case: welding of an attached flange of an integral C-frame onto a thermoplastic skin laminate.

Resistance welding uses joule heating of an electrically conductive implant or welding conductor caused by a flow of an electrical current. The welding element consisting of the welding conductor and additional electrical insulation sheets is placed in between the welding components and generates the heat at the interface. The temperature is increased towards the processing temperature (T_p), while a weld pressure of at least 0.5 MPa assures adequate consolidation of the bondline. Since the heating rate, target temperature level and cooling rate can be adjusted by the power input, the possibility for a multi-stage welding guidance is given and can be used for an optimization of the joint strength.

2. Weld process definition and optimization procedure

2.1 Resistance welding setup and functionality

A weld module (see Figure 1) - comparable to those later used on the full-scale welding tool for attached flange joining - was designed and validated on our resistance welding test bench in order to optimize the processing parameters. The weld module itself consists of the following main components: pneumatic cylinder (1) for applying weld pressure and contact pressure, lever arm (2) with a transmission ratio of 1:4 (piston pressure to welding pressure), disk spring package (3) to ensure a relative movement between welding pressure piece (4) and the copper contacting blocks (5). The process sequence was defined within the software TopControl, which was used to control the power supply (Regatron TopCon Quattro).

The corresponding measurement data of welding pressure, current and voltage levels as well as the bondline temperature were recorded and merged via an in-house developed quality assurance software.
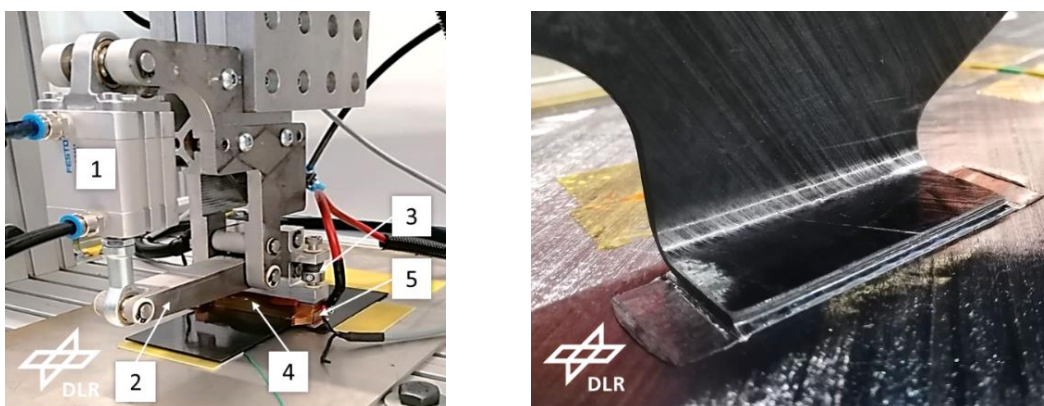

Figure 1 Weld module (left) for performance validation and process parameter definition/ optimization. Full-scale process verification of a resistance-welded C-frame cutout on an in-situ T-AFP skin laminate (right).

Figure 1 (left) shows the weld module used for process parameter identification and optimization. The right-hand side picture highlights a cutout of the later use case, a welded attached flange of an integral C-frame.

For process definition 2.76 mm thick, flat, press-consolidated laminates of the stacking sequence [45°,135°,90°,0°,135°,45°,45°,90°,135°,45°,135°,0°,90°,135°,45°] were welded with an overall weld length of 84 mm and an overlap of 22 mm in single lap shear (SLS) configuration. This stacking sequence is attributed to the later use case. The organosheets 0°-axis was aligned with the axis of force application. Within this study two different types of welding elements, configuration A with pre-consolidated glassfiber (GF)/LM-PAEK insulation (Toray 4HS, EC5 E-glass prepreg, 105gsm) and configuration B with a 100 µm LM-PAEK film insulation (Victrex APTIV AE™ Film 6013-AEG-100), were used. Toray`s pre-consolidated 5HS, T300JB carbon woven prepreg, 277gsm was chosen as welding conductor. A thermocouple type K placed in the center of the bondline between bottom organosheet and welding element provided temperature feedback during the weld process.

2.2 Water-coupled ultrasonic inspection

Resistance welding technology, based on a carbonfiber welding element, offers the possibility of applying non-destructive testing (NDT) methods, which are conventionally deployed for testing integral structures, since a mono-material composite is produced during assembly. In order to check for non-conformance indications and bondline homogeneity, the standard NDT method water-coupled ultrasonic scanning (WUS) according to AITM6-4010 was chosen. An OLYMPUS OmniScan® SX phased array flaw detector with 5L64-NW1 probe and SNW1-OL-IHC wedge were used to measure the ultrasonic data. Here, the probe was mounted on a 2-axis GLIDER X-Y scanner to allow insightful evaluation of the A-, B- and C- Scans.
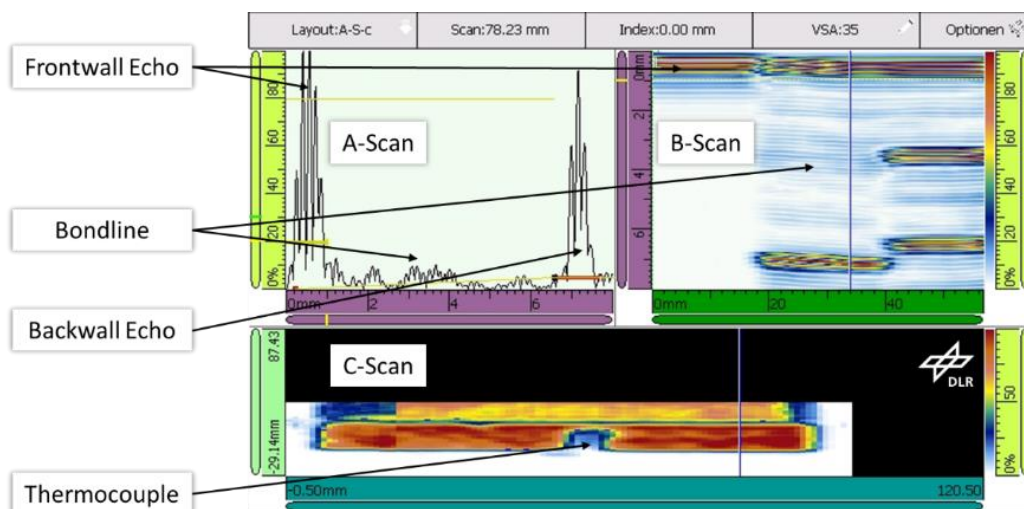

Figure 2 Representative water-coupled ultrasonic scan result of a resistance welded coupon in SLS configuration

The capability of producing completely closed and homogeneous welds by resistance welding is represented within the scan of Figure 2. Here, an 84 mm x 22 mm bondline corresponding to the above described weld setup was achieved. A-, B- and C-Scans highlight a perfect weld quality over the entire bondline indicated by the damping of the amplitude color-coded in red, comparable to an integral composite structure. The damping losses in the center of the bondline marked in blue are attributed to the thermocouple and its Polyimide insulation. Results of the WUS were used for a quantitative comparison of the welding quality and definition of the later DoE input parameter boundaries.
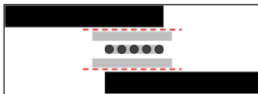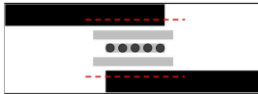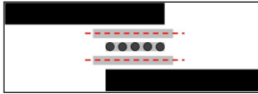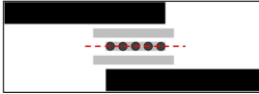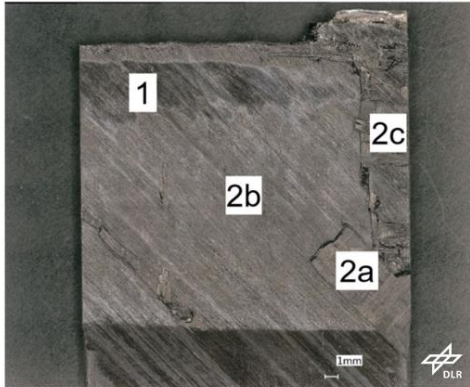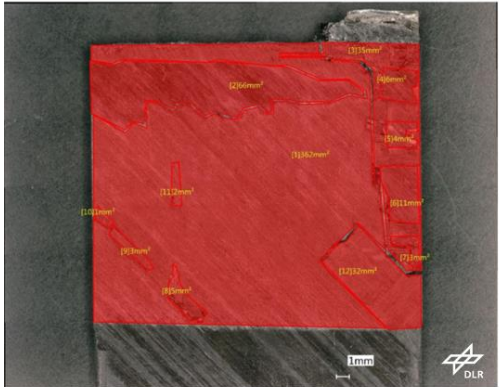
2.3 Coupon preparation and destructive testing

Each welded specimen was cut into three 25.4 mm wide SLS coupons by a waterjet cutter. In comparison to the standard-compliant tests (according to DIN-EN 2243-1/ AITM1-0019) of an overlap length of 12.5 mm, the entire welding width of 22 mm was used for testing without further preparation, like notching, well knowing that the increased joint overlap would result in a superimposed tensile peel load. The reason was the need to gain knowledge about the bearable fracture load of the entire welded joint. In particular, since it was expected that the effects of lower welding temperature values would especially affect the joint strength at the edges. The mechanical testing of the coupons was performed at PAG`s aerospace certified structural lab. Aluminum tabs were used to compensate for the eccentricity of the coupons at clamping in the tensile testing machine (Zwick BTC Z100 & Pulser P40). The testing was performed at a test speed of 3500 N/min, clamping length according to AITM1-00019 (112,5 - 127) mm at 24.5 °C and 33.7 % rel. humidity. [1]

2.4 Microscopic fracture surface analyses

Following the SLS test, a comprehensive fracture surface analysis was performed to gain insight into the dependence on process control during welding and its influence on the fracture pattern. For this purpose, the fracture surfaces were imaged in reflected light microscopy using a Keyence VHX-5000 microscope. Four fracture zones (ID_1 and ID_2a-c) were defined to allow an exact assignment of the fracture surface fractions to failure location (see Table 1).

Table 1 Schematic and physical fracture classification [2]

The respective fracture fractions were characterized optically under the digital microscope and measured geometrically using the polygonal tension function. Fracture ID_1 is characterizing a bondline separation between the welding elements insulation and the organosheet and indicates a too low weld temperature level. At Fracture ID_2a-c the crack propagates through one of the semi-finished products organosheet (ID_2a), welding element insulation (ID_2b) or the electrical conductor (ID_2c).

3. Design of Experiments

3.1 Model description

Design Expert®, a DoE software was used to plan and evaluate the test series. In order to reduce the overall welding and testing effort and still demonstrate the multifactorial interactions a Face-Centered Central Composite Design (FCCCD) was used. The FCCCD is a response surface method and spans its experimental space as a combination of cube and star. This allows to detect up to quadratic terms. In order to obtain a sufficient statistical validation of the test results, the center point was repeated six times, and the corner and star points of the test room were repeated twice. At each of the test points at least two specimens were welded, containing the described number of three coupons.

3.2 Input parameters, constants and responses

In this study, the influence of the joining parameters on the fracture load as well as the fracture behavior were investigated in detail. The process was designed in two distinct phases. In the first phase, the welding element should be heated first above the melting temperature of the thermoplastic matrix to the final T_P. In the second phase, the voltage and thus the temperature is reduced to allow post-crystallization at about 220 °C. The main influence on the responses were expected in the dwell time above the crystallite melting temperature (represented by the combination of Phase_1 Weld Voltage and Phase_1 Weld Duration), as well as the cooling rate during post-crystallization (represented by the combination of Phase_2 Weld Voltage and Phase_2 Weld Duration). These factors were set as input parameters for the DoE and varied in between the boundaries. The welds were performed in constant voltage mode.

Table 2 Input parameters and their variable ranges within the scope of the performed DoE

Factors/ Input Parameters	Design Points	Unit
Phase_1 Weld Voltage	23 | 25 | 27	V
Phase_1 Weld Duration	20 | 25 | 30	s
Phase_2 Weld Voltage	18 | 19 | 20	V
Phase_2 Weld Duration	5 | 10 | 20	s

The design points shown in Table 2 were determined during preliminary tests [3], [2]. In Phase_1, the voltage-time combinations were designed for a targeted processing temperature range between 305 °C (T_m) and 400 °C. Since the T_P-range of LM-PAEK is at (340-385) °C [4] the upper temperature limit was defined not to extraordinary exceed these limits and to remain below the degradation temperature (T_{d_PEEK} = 520 °C) [5]. During preliminary welding experiments a temperature drop of about 36°C/s, linear approximated from voltage shut down at 360 °C to 220 °C (temperature of maximized crystallization rate) was investigated. In comparison with Differential Scanning Calometry (DSC) measurements from literature [5], [6], the necessity for lower cooling rates was confirmed in order to increase the crystallinity content. For this purpose, the welding Phase_2 was implemented into the process cycle. The Phase_2 Voltage levels were selected to meet a bondline target temperature range of (220-270) °C.

Besides the described DoE variables, the remaining process parameters like contact pressure, weld pressure and the kind of contact preparation were kept constant on a pre-investigated optimum during this trial series. The parameters fracture load [N], failure mode (ID_1, 2a-c), fracture surface (according to fracture ID as %-value of the overall weld surface) and the maximum processing temperature [°C] were defined as responses of the DoE.

4. Results, interpretation and optimization

4.1 Stage one welding element (GF-based insulation)

The Analysis of Variance (ANOVA) within Design Expert® showed statistically significant influences of the parameters Phase_1 Weld Voltage and Phase_1 Weld Duration on the fracture load. Figure 3 shows the influences of the Phase_1 input parameters on the fracture load, highlighting a major impact due to a voltage increase compared to an extension of the weld duration. This indicates the stronger dependence of the processing temperature as compared to the dwell time.
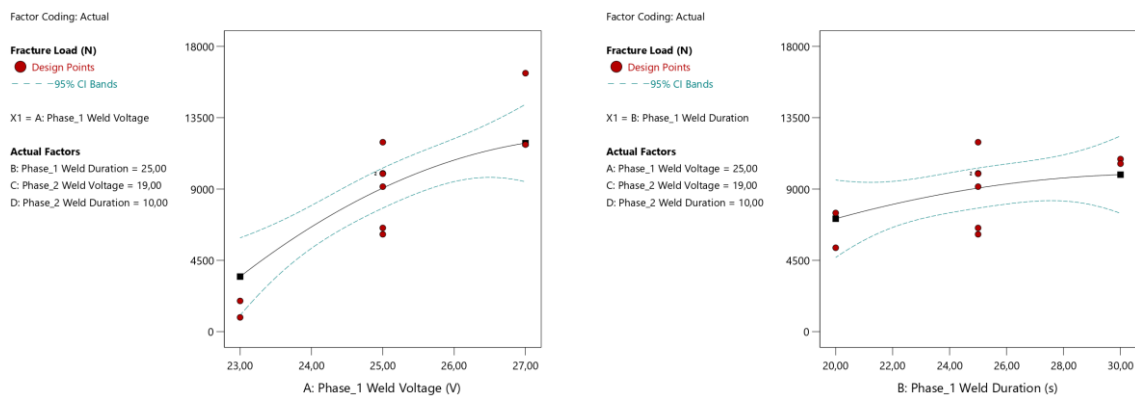

Figure 3 Influence of Phase_1 Weld Voltage (left) and Phase_1 Weld Duration (right) on the bearable fracture load

Fracture surface analyses post to destructive testing exhibited a mixed-mode failure of each specimen with the highest fracture surface percentage in failure mode ID_2b (85.15 %), followed by the failure modes ID_2a (12.23 %), ID_1 (2.46 %) and ID_2c_0.16 %. Since in between the failure modes 2a-c, no valuable impact on the fracture load level was observed, those three ID`s have been summarized to an overall ID_2. In the further course the evaluation, the responses failure mode and fracture surface have been combined to the response percentage of area in failure ID_2, due its higher expressiveness. Here, the occurrence of failure mode ID_1 was exclusively attributed to Phase_1 Weld Voltage levels lower than 24.1 V, leading to weld temperature levels below 330 °C and is thus outside the processing specification.

A comparison of the responses fracture load (Figure 3) and the percentage of area in failure ID_2 (Figure 4), clearly shows that the increase in fracture load is caused by an increase in the welded area due to an elevated maximum processing temperature and is not majorly influenced by a prolonged Phase_1 Weld Duration. Furthermore, an extension of the Phase_1 Weld Duration did not show any significant influence on the shift of the fracture type from ID_1 to ID_2.
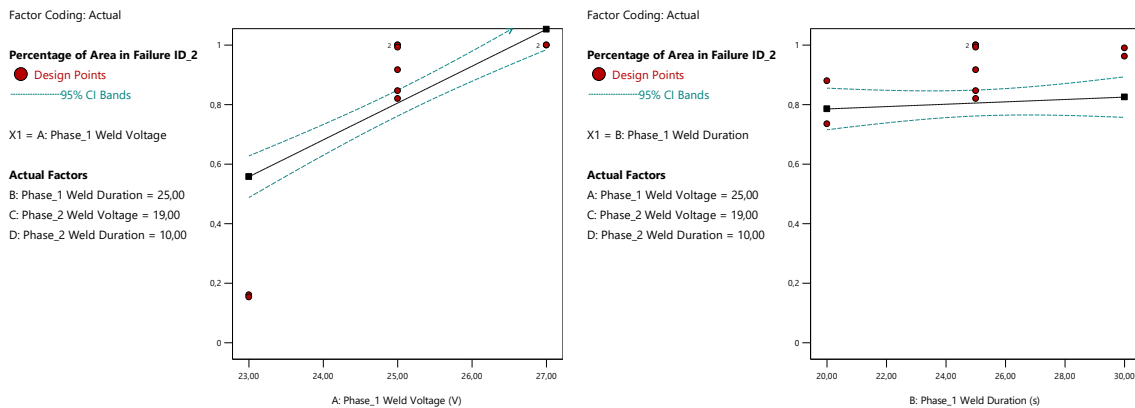
Figure 4 Influence of Phase_1 Weld Voltage (left) and Phase_1 Weld Duration (right) on the percentage of area in failure ID_2

The impact of the second weld phase which should reduce the cooling rate and thus increase the crystallinity content highlights, compared to first weld phase, a minor impact on the overall fracture load (see Figure 5) within the investigated design space. Since the bearable fracture load increases towards the edge of the design space for the first weld phase (longer weld duration at higher voltage levels) it cannot be assured, that the fracture load optimum is located within the chosen design space. However, the design space meets the superordinate criterion on process robustness and reliability. Related to the second weld phase it can be concluded, that a minor increase in the fracture load can be achieved by an increased Phase_2 Weld Duration in combination with a low Phase_2 Weld Voltage level.
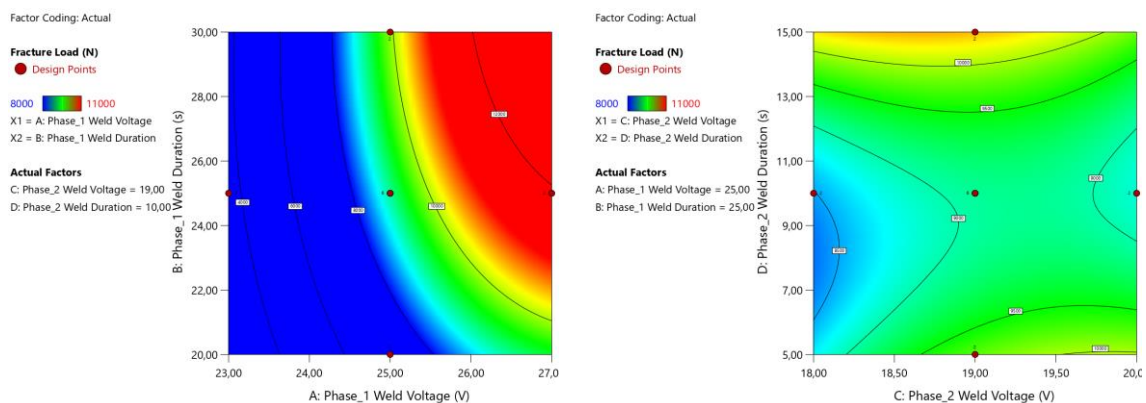

Figure 5 Comparison of the impact of the first (left) and second (right) weld phase on the fracture load.

In order to define a valuable set of input parameter combinations for the described use case (frame integration) a parameter optimization was performed. A maximization of the fracture load (importance: ++++) and percentage of failure area in ID_2 (importance +++), as well as target maximum temperature level within the scope range of T_P (340-385) °C were defined as boundary conditions. The results of the most desirable numerical optimization are plotted within Figure 6, confirming the above concluded suggestion on defining the first welding phase towards the upper right corner and the second phase towards the upper left corner (compare Figure 5) of the design space, i.e. applying maximum voltage of 27 V for 30 s in the first weld phase, whilst in Phase_2 the voltage level is reduced to 19 V for a dwell time of 15 s.
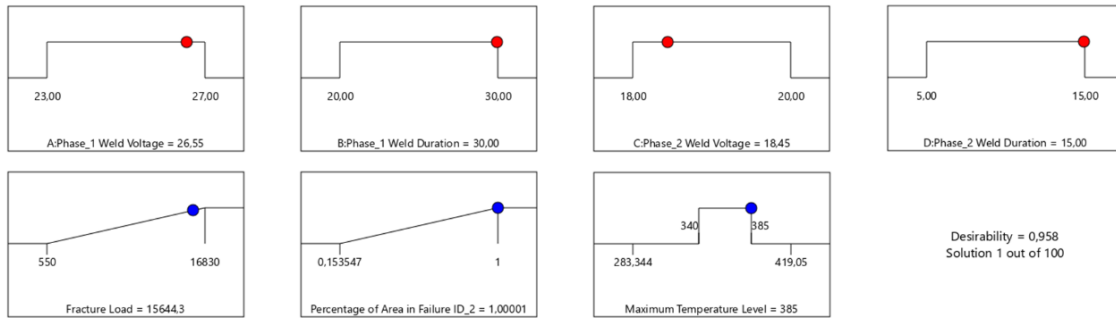
Figure 6 Results of the numerical optimization of the welding parameters for CF/LM-PAEK.

The numerical optimization predicts under assignment of the suggested input parameter combination a resulting fracture load of 15664.3 N at a percentage of area in failure ID_2 of 100 % and a maximum temperature of 385 °C in the bondline.

The proposed parameter combination of 26.6 V for 30 s in the first and 18.5 V for 15 s in the second welding stage was subsequently validated on eight tested specimen and showed with a fracture load of (15795 ± 1089) N a highly precise conformance on the predicted value.

4.2 Stage two welding element (APTIV-based insulation)

A further optimization towards higher fracture loads was made by replacing the GF/LM-PAEK insulation by a pure matrix film. Since the tests were carried out in parallel with the mechanical testing of the specimens from the DoE, the optimized parameter set could not be used here. Furthermore, the possibility of a two-stage weld pressure application (low pressure of 1.2 bar during Phase_1; high pressure of 8.1 bar applied at Phase_1 Voltage shutdown) was implemented in order to reduce the conductor squeeze out during the heating phase and prevent from local overheating and current leakage.
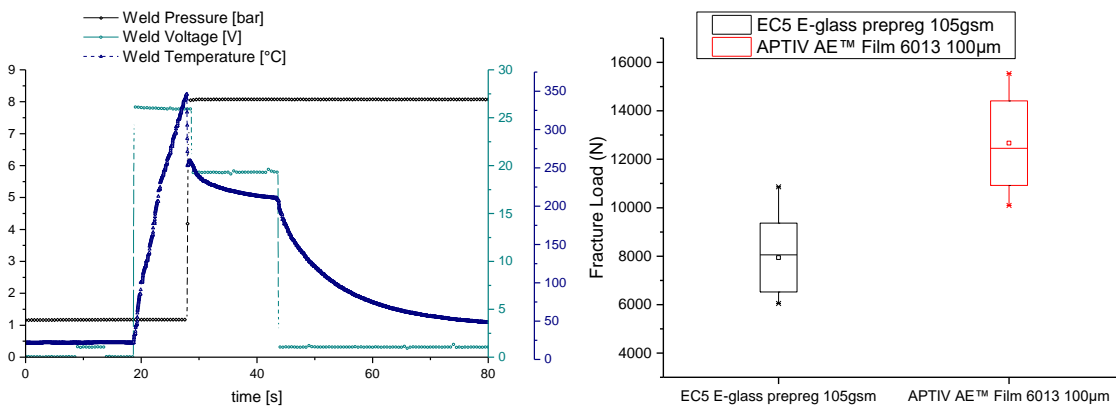

Figure 7 Adapted, non-optimized welding process for increased process robustness at reduced conductor squeeze out (left). Potential increase of fracture load due to replacement of the GF-based insulation by a neat resin film (right).

Figure 7 (left) shows the processing parameters over time for a 27 V/10 s first weld phase and a 20 V/15 s second weld phase process sequence and additional possibility of increasing the weld performance. Since the potential for an increase in mechanical performance could already be shown for a non-optimized parameter set, further investigations are currently being carried out to determine the absolute fracture load increase, based on the optimized weld parameter set.

5. Summary and Conclusion

Within this paper we present our research activities on the resistance welding technology maturation within the scope of the MFFD upper shell development. For the final all-thermoplastic composite fuselage C-frames shall be welded to the in-situ consolidated skin. The conducted experimental investigations are based on pre-consolidated TC 1225 LM-PAEK laminates provided by TORAY. A custom-made weld module comparable to the final application was used for coupon welding of single lap shear specimen at varying weld parameters defined by design of experiment. The resulting sample quality was determined by WUS inspection, SLS testing and fracture surface analysis. By statistical analysis of the FCCCD an optimum for welding was found with a first stage heating the weld element by applying a voltage of 26.6 V for 30 s. In the second stage, the cooling rate is reduced by applying a voltage of 18.5 V for 15 s so that re-crystallization is promoted at temperatures above 220 °C. The validation of the welding input parameters, provided by the numerical optimization showed good conformance with the validated fracture load values.

Recent investigations have indicated that resistance welding, based on a welding element with a carbonfiber conductor and without glass insulation but a neat resin film may also be a viable opportunity, further reducing the amount of foreign material in the weld seams.

Acknowledgements

Disclaimer

The results, opinions, conclusions, etc. presented in this work are those of the author(s) only and do not necessarily represent the position of the JU; the JU is not responsible for any use made of the information contained herein.

6. References

[1] V. Gadletz, T. Lehl, and G. Knopp, "TP-WL1413-MFFD SLS DLR_V3 Test Protocol," Premium Aerotec GmbH, May 2021.

[2] A. Thomé, "Ermittlung und Validierung der Prozessgrößen beim elektrischen Widerstandsschweißen von faserverstärkten Hochleistungsthermoplasten und deren Einfluss auf die Verbindungsqualität," Institute of Structures and Design (IBT), German Aerospace Center (DLR), Augsburg, Sep. 2021.

[3] M. Endrass, M. Engelschall, S. Jarka, S. Bauer, and F. Fischer, "Deliverable D2.1.8-55 (DEK), Optimization of welding parameters of LM PAEK," Clean Sky 2, D2.1.8-55, Dec. 2020.

[4] Toray, "Toray Cetex TC1225," Toray Advanced Composites, G. van der Muelenweg 2 7443 RE Nijverdal, The Netherlands, 2020.

[5] J. Audoit, L. Rivière, J. Dandurand, A. Lonjon, E. Dantras, and C. Lacabanne, "Thermal, mechanical and dielectric behaviour of poly(aryl ether ketone) with low melting temperature," *Journal of Thermal Analysis and Calorimetry*, vol. 135, no. 4, pp. 2147–2157, Apr. 2018.

[6] I. Schiel, L. Raps, A. R. Chadwick, I. Schmidt, M. Simone, and S. Nowotny, "An investigation of in-situ AFP process parameters using CF/LM-PAEK," *Advanced Manufacturing: Polymer & Composites Science*, vol. 6, no. 4, pp. 191–197, Oct. 2020.